

Est.
1841

YORK
ST JOHN
UNIVERSITY

Francis, Leslie J. ORCID logoORCID:
<https://orcid.org/0000-0003-2946-9980> and Village, Andrew ORCID
logoORCID: <https://orcid.org/0000-0002-2174-8822> (2021) Reading
the Church of England's Response to the Covid-19 Crisis: The
Diverging Views of Anglo-Catholic and Evangelical Clergy. *Journal
of Anglican Studies*, 20 (2). pp. 185-197.

Downloaded from: <https://ray.yorks.ac.uk/id/eprint/5575/>

The version presented here may differ from the published version or version of record. If
you intend to cite from the work you are advised to consult the publisher's version:
<http://dx.doi.org/10.1017/S1740355321000267>

Research at York St John (RaY) is an institutional repository. It supports the principles of
open access by making the research outputs of the University available in digital form.
Copyright of the items stored in RaY reside with the authors and/or other copyright
owners. Users may access full text items free of charge, and may download a copy for
private study or non-commercial research. For further reuse terms, see licence terms
governing individual outputs. [Institutional Repository Policy Statement](#)

RaY

Research at the University of York St John

For more information please contact RaY at ray@yorks.ac.uk

1 **Utilization of coal fly ash waste for effective recapture of phosphorus**
2 **from waters**

3 Rui Xu ^{1,2}, Tao Lyu ^{*3}, Lijing Wang ⁴, Yuting Yuan ⁵, Meiyi Zhang ⁶, Mick Cooper ⁷,
4 Robert J.G. Mortimer ^{8,9}, Queping Yang ^{1,2}, Gang Pan ^{*6,7,9}

5 ¹ *Chinese Research Academy of Environmental Sciences, Beijing 100012, China*

6 ² *National Joint Research Center for Yangtze River Conservation, Beijing 100012, China*

7 ³ *Cranfield Water Science Institute, Cranfield University, College Road, Cranfield,*
8 *Bedfordshire MK43 0AL, United Kingdom*

9 ⁴ *College of Resources and Environment, University of Chinese Academy of Sciences, Beijing*
10 *100049, China*

11 ⁵ *UNSW Water Research Centre, School of Civil and Environmental Engineering, The*
12 *University of New South Wales, Sydney, NSW 2052, Australia*

13 ⁶ *Research Center for Eco-Environmental Sciences, Chinese Academy of Sciences, Beijing*
14 *100085, China*

15 ⁷ *School of Animal, Rural and Environmental Sciences, Nottingham Trent University,*
16 *Brackenhurst Campus, Nottinghamshire NG25 0QF, United Kingdom*

17 ⁸ *School of Humanities, York St John University, Lord Mayor's Walk, York YO31 7EX, United*
18 *Kingdom*

19 ⁹ *Nanjing Xianglai Academy of Eco-environmental Science and Technology, Nanjing 210046,*
20 *China*

21 **Corresponding authors: gang.pan@ntu.ac.uk (G.P.), t.lyu@cranfield.ac.uk (T.L.)*

22

23 **Abstract**

24 Reutilisation of the waste by-products from industrial and agricultural activities is
25 crucially important towards attainment of environmental sustainability and the
26 'circular economy'. In this study, we have developed and evaluated a sustainably-
27 sourced adsorbent from coal fly ash, which was modified by a small amount of
28 lanthanum (La-FA), for the recapture of phosphorous (P) from both synthetic and real
29 natural waters. The prepared La-FA adsorbent possessed typical characteristic
30 diffraction peaks similar to zeolite type Na-P1, and the BET surface area of La-FA was
31 measured to be 10.9 times higher than that of the original FA. Investigation of P
32 adsorption capability indicated that the maximum adsorption (10.8 mg P g^{-1}) was 6.14
33 times higher than that (1.8 mg P g^{-1}) of the original fly ash material. The ζ potentials
34 measurement and P K-edge X-ray Absorption Near Edge Structure (XANES) spectra
35 demonstrated that P was bonded on La-FA surfaces via an adsorption mechanism. After
36 applying the proposed adsorbent to real lake water with La/P molar ratios in the range
37 from 0.5:1 to 3:1, the La-FA adsorbent showed the highest phosphate removal ability
38 with a La/P molar ratio 1:1, and the P adsorption was similar to that performance with
39 the synthetic solution. Moreover, the La-FA adsorbent produced a negligible effect on
40 the concentrations of total dissolved nitrogen (TDN), $\text{NH}_4^+\text{-N}$ and $\text{NO}_3^-\text{-N}$ in water.
41 This study thus provides a potential material for effective P recapture and details of its
42 operation.

43 **Keywords:** Circular economy; coal fly ash; eutrophication management, lanthanum
44 modification; phosphorus adsorbent

45 **1. Introduction**

46 Along with the growth in global population and concurrent industrialization, the
47 widespread application of phosphorus (P) as fertilizer and animal feed have resulted in
48 substantially increased discharge of P into the environment and intensified episodes of
49 eutrophication in natural waters (Conley et al., 2009; Pan et al., 2018; Smith et al.,
50 1999). It has been reported that eutrophication could even occur at P concentrations as
51 low as 0.02 mg P L⁻¹ (Fernandez et al., 2007). Traditional and enhanced processes for
52 the biological removal of P during natural and waste water treatments are generally not
53 able to sustainably achieve such low effluent P concentrations (Kumar et al., 2019). The
54 dosing of aluminium- or iron-based salts is a common approach in sewage treatment
55 plants in order to secure an ultra-low level effluent with respect to P (Nakarmi et al.,
56 2020; White et al., 2021). However, as P is a non-renewable resource, not only removal,
57 but also recovery and recapture of the discharged P is strategically important for
58 environmental sustainability (Pan et al., 2020). Therefore, treatment by adsorption is
59 often suggested, due to the multiple advantages of low carbon footprint, minimal waste
60 generation and the further option for P recovery (Kang et al., 2003).

61 Various synthetic adsorbents for P have been developed, and the valorisation of waste
62 by-products from industrial and agricultural activities has recently drawn substantial
63 attention within the concept of the circular economy (Zamparas et al., 2020). Many raw
64 solid wastes (Table 1), such as steel slag (Bowden et al., 2009), magnesite dust (Al-
65 Mallahi et al., 2020), concrete powder (Liu et al., 2020), and fine-grained by-products
66 (Kasprzyk et al., 2021), have been investigated for P removal. In addition to the

67 immediate advantage of low cost, some of these materials possess high porosity and
68 mineral mixtures consisting of aluminium and other metal oxides, and have yielded P
69 removal capabilities comparable to those of synthetic adsorbents. As coal combustion
70 is still one of the most important sources of energy, the global generation of fly ash is
71 estimated to be approximately 750 million tons, and thus the treatment/utilisation of
72 these wastes is crucial (Blissett & Rowson, 2012). It is necessary to find a feasible way
73 for the utilization of fly ash. Additionally, the complexity and variety of fly ash should
74 also be taken into consideration since it comprised of hundreds of different individual
75 minerals and mineral groups (Vassilev and Vassileva, 2005).

76 Currently, researchers have attempted to use the raw fly ash for P removal. Some
77 approaches have been used to improve the removal ability of modified fly ash through
78 pre-treatment of acid/alkaline solutions and modification by metal ions (Hermassi et al.,
79 2020). Although the modified fly ash could achieve P adsorption from several to
80 hundreds of mg P g⁻¹ (Li et al., 2006; Wang et al., 2016b), it is considered that the
81 overall efficiency could be improved further. The use of lanthanum (La), an
82 environmentally friendly and relatively abundant rare earth element, is currently being
83 used commercially to synthesise the P adsorbent *Phoslock*[®]. As a modifier on bentonite
84 for P removal, a small portion of La (*ca.* 5.6%) could lead to P adsorption up to 10.6
85 mg P g⁻¹ due to its excellent P-binding ability (Haghseresht et al., 2009). A La-based P
86 adsorbent could also overcome adverse effects of fluctuating pH and redox conditions
87 in solution, attributable to strong P binding reactions (Wang et al., 2016b; Shin et al.,
88 2005; Zhang et al., 2016), however, research into the use of La as modifier on fly ash

89 for P removal is still not sufficient. It is therefore hypothesised that fly ash doped with
90 a relatively small amount of La would result in a superior, low cost, and
91 environmentally-friendly P adsorbent.

92 In many experiments demonstrating novel P adsorbents, adsorption capabilities are
93 invariably tested using a synthetic P-contaminated solution with initial concentrations
94 ranging from tens to hundreds mg P L⁻¹ (Xu et al., 2020). However, the P concentrations
95 in natural waters or sewage effluent from upstream biological/chemical P removal
96 treatments are usually much lower, for example in the range 0.1-1.0 mg P L⁻¹ (Wang et
97 al., 2016a). Moreover, the removal efficiency of P from real waters could be affected
98 by the presence of competing ions, such as SO₄²⁻ and CO₃²⁻ (Dithmer et al., 2016; Zhang
99 et al., 2016). Previous studies, shown in Table 1, have reported a *ca.* 10% lower P
100 removal ability from real wastewaters compared with that obtained from synthetic
101 wastewater under the same condition. When targeting a real-life deployment, it should
102 be realised that little is known about the behaviour and mechanisms of P removal by
103 the proposed La-modified fly ash adsorbent from both synthetic and natural real waters.

104 In order to address these knowledge gaps, the aims of this study were to develop a La-
105 modified adsorbent from solid waste coal fly ash and to investigate its performance for
106 P recapture from examples of both synthetic and real waters. Adsorption capacity,
107 kinetics and isotherm characteristics, and the effect of pH on P adsorption, were initially
108 investigated with synthetic water samples. The P K-edge X-ray Absorption Near Edge
109 Structure (XANES) technique was employed to explore and characterise the

110 microstructures formed when P bonded onto the proposed adsorbent. Moreover, the P
111 removal performance of this material was also investigated with real lake waters, in
112 order to provide an evidence, base that can be referenced regarding further
113 implementations.

114 **Table 1.** Summary of the performance of various waste materials for P removal.

Material	Experiment solution	Dosage (g L ⁻¹)	pH	Initial P (mg P L ⁻¹)	P removal (%)	P adsorption capacity (mg P g ⁻¹)	Reference
Fly ash	Synthetic	2	3-11	30-300	100	-	(Shuai Gu et al., 2021)
	Real	2	-	51.5	100	-	
Steel slag	Synthetic	40	-	0-100	>90	1.14-2.49	(Barca et al., 2012)
	Real	40	-	0.41-1.11	>90	0.14-2.50	
	Synthetic	-	2-12	1-50, 100-300	62	8.39	(Bowden et al., 2009)
Eggshell	Synthetic	20	-	0.5-3.0	90	121	(Torit & Pihusut, 2019)
	Real	50	7.3	1.7	80	-	
	Synthetic	0.96	-	-	96.2	3.32	(Cy & Lpv, 2019)
Mussel shell	Synthetic	0-80	1.5-9.5	0-20	-	6.95	(Xiong et al., 2011)
Oyster shell	Synthetic	6	7.0-12	11.9	98	-	(Lee et al., 2009)
	Synthetic	400	-	6-80	-	32.9	(Wang et al., 2013)
Orange waste gel (loaded with zirconium)	Synthetic	1.67	1-9	-	-	57	(Biswas et al., 2008)
Magnesite dust	Synthetic	22.2	9	665	63%	-	(Al-Mallahi et al., 2020)
Concrete powder	Synthetic	-	10.5	20	-	4.96	(Liu et al., 2020)
Broken bricks	Synthetic	400	-	6-80	-	0.59	(Wang et al., 2013)
Iron humate	Synthetic	10-40	-	3.1-124	-	3.4-11.5	(Jano et al., 2011)
Fine-grained by-product	Synthetic	10	-	97.3	97.8	9.58	(Kasprzyk et al., 2021)

115

116 **2. Materials and methods**

117 **2.1. Material preparation and characterisation**

118 Raw coal fly ash (FA) was obtained from a power plant in Datong City (Shanxi province,
119 China). The ash was washed three times with deionized water, dried at 105 °C, then
120 passed through a 180 mesh sieve before use. La-modified fly ash (La-FA) was
121 synthesized by the following process. The FA was first treated with 2.0 mol L⁻¹ NaOH
122 solution at 95 °C for 24 h at a liquid/solid ratio of 360 mL alkali solution per 60 g FA,
123 to obtain the zeolite and waste alkaline solution. After cooling to about 25 °C, a LaCl₃
124 solution (0.23 mol L⁻¹, 100 mL) was added dropwise to the mixture with continuous
125 stirring, and the mixture further stirred for another 4 h at 25 °C. Finally, the resulting
126 solid was washed three times with deionized water and freeze-dried over 24 h.

127 To obtain the exact content of La in the prepared La-FA, samples were digested in HF-
128 HClO₄-HNO₃ solution and the chemistry of each resultant solution was determined by
129 inductively coupled plasma optical emission spectrometry (ICP-OES, Optima 8300,
130 PerkinElmer, USA). The morphologies of the raw FA and La-FA materials were
131 observed by field emission scanning electron microscopy (FESEM, SU 8020, Hitachi,
132 Japan). X-ray powder diffraction patterns were recorded on an X'Pert PRO MPD X-
133 ray diffractometer (Malvern Panalytical, The Netherlands) with Cu-K radiation ($\lambda =$
134 1.5408) at 40 kV and 40 mA in the 2θ range of 5° to 90°. Brunauer-Emmett-Teller (BET)
135 surface areas and pore size distributions were examined by a Micromeritics ASAP 2020
136 static volumetric analyser (Micromeritics Instrument Corp., Norcross, USA). Zeta (ζ)
137 potential analysis of samples was performed by Zetasizer Nano ZS potential analyzer

138 (Malvern Panalytical Ltd., United Kingdom).

139 **2.2. P adsorption experiment**

140 **2.2.1. Adsorption isotherm**

141 P adsorption isotherm experiments were conducted in 50 mL polypropylene tubes.
142 Samples of FA and La-FA (1.0 g L⁻¹) were mixed with solutions containing various
143 concentrations of KH₂PO₄ each with 0.01 mol L⁻¹ NaCl ionic background. The solution
144 pH was adjusted to 8.50 ± 0.05 with 0.01 mol L⁻¹ HCl and NaOH. The suspensions were
145 shaken at 25 °C for 48 h. The suspensions were then centrifuged, filtered through 0.45
146 µm membrane filters, and the clear supernatants used to determine P concentrations by
147 the ascorbic acid method, using a UV-756 PC spectrophotometer at 880 nm (Shanghai
148 Sunny Hengping Scientific Instrument Co. Ltd., China).

149 In order to model the adsorption results, Langmuir (Eq. 1) and Freundlich (Eq. 2)
150 isotherms were used in this study, respectively.

$$151 \quad q_e = \frac{q_m k_L C_e}{1 + k_L C_e} \quad (1)$$

$$152 \quad q_e = K_F C_e^{1/n} \quad (2)$$

153 *Where q_e is the equilibrium adsorption capacity (mg g⁻¹), q_m refers to the maximum adsorption*
154 *capacity (mg g⁻¹), C_e is the equilibrium concentration after adsorption (mg L⁻¹), K_L is the*
155 *constant in Langmuir model (L mg⁻¹), K_F is the constant in Freundlich model (mg g⁻¹), n is the*
156 *constant in Freundlich isotherm model representing adsorption intensity.*

157 **2.2.2. Adsorption kinetics and desorption experiments**

158 Adsorption kinetic experiments were carried out in 1000 mL flasks containing 500 mL

159 P solution with concentrations of 10 and 30 mg P L⁻¹, and 0.5 g adsorbent samples
160 added. The flasks were shaken at 25 °C for 48 h at 170 rpm. About 0.5 mL of each
161 supernatant was sampled at various time intervals in order to determine P concentration.
162 The pH was maintained at 8.50 ± 0.05 during the 48 h equilibration time.

163 Pseudo-second order kinetics (Eq. 3) and intra-particle diffusion (Eq. 4) models were
164 used to model the experimental data, respectively.

$$165 \quad \frac{t}{q_t} = \frac{1}{k_2 q_e^2} + \frac{t}{q_e} \quad (3)$$

$$166 \quad q_t = k_i t^{1/2} \quad (4)$$

167 *Where q_e and q_t represents the equilibrium capacity (mg g⁻¹) and adsorption amount versus*
168 *time t (min), k_2 is the equilibrium rate constant of pseudo-second-order adsorption (g mg⁻¹ h⁻¹),*
169 *k_i is the rate constant of intra-particle diffusion model (mg g⁻¹ h^{-1/2}).*

170 At the conclusion of the adsorption kinetics experiment, the exhausted solutions of La-
171 FA samples with initial P concentration 30 mg P L⁻¹ were first centrifuged, and 10 mL
172 of the suspension at the bottom were preserved, then NaCl solution (0.01 mol L⁻¹) was
173 added in order to maintain the same ionic strength. The suspensions were then shaken
174 at 25 °C for 48 h. After that, the P concentrations of the clear supernatants were
175 measured in order to determine the P desorption ability of the adsorbent.

176 **2.3. The effect of pH on P removal**

177 In order to assess the effect of pH on the equilibrium adsorption capacity, adsorption of
178 P onto La-FA was conducted at pH 4, 5, 6, 7, 8, 9, and 10. La-FA (1.0 g L⁻¹) was added
179 to 50 mL polypropylene tubes with an initial P concentration of 30 mg P L⁻¹ with NaCl

180 (0.01 mol L⁻¹) ionic background, and shaken at 170 rpm at 25 °C for 48 h. The solution
181 pH was maintained with 0.01 mol L⁻¹ HCl and NaOH.

182 **2.4. P K-edge XANES data collection and analysis**

183 The P K-edge XANES data were collected in fluorescence yield mode on Beamline
184 4B7A at the Beijing Synchrotron Radiation Facility (BSRF), China. Measurements
185 were acquired at energies between -30 to +90 eV relative to P K-edge energy of 2152
186 eV with a minimum step size of 0.3 eV over the range 2140 and 2180 eV. XANES
187 spectra of samples were normalized by the ATHENA software program (Ravel &
188 Newville, 2005).

189 **2.5. P binding experiments in real lake water**

190 Real lake water was collected from Meiliang Bay of Taihu Lake (Jiangsu province,
191 China) in November 2017. Taihu Lake is a mild eutrophic surface water and
192 experiences periodic algal blooms every few years (Pan et al., 2019). In total, 5.0 L
193 sample was collected by a plexiglass water sampler (Bei Jing Gresp Co., Ltd, China)
194 from 0.5 m deep below the surface in the centre of Meiliang Bay (31°43'N, 120°14'E).
195 The water sample was first screened by a 180 µm mesh to remove large zooplankton
196 grazers and then stored under 4 °C before being used for the following experiment. The
197 chemical characteristics of the lake water are listed in Table 2. Stock suspensions of La-
198 FA were prepared by continuous mixing of the adsorbent materials (50 mg) with
199 deionized water (500 mL). Subsamples of 0.3, 0.6, 1.2, 1.8 and 2.4 mL were taken from
200 these suspensions to obtain the desired adsorbent dosages, and then transferred to 50

201 mL polypropylene tubes containing lake water samples (40 mL) previously filtered
 202 through 0.45 μm membrane filters. The final volume of each solution was maintained
 203 at 45 mL by addition of aliquots of real lake water. The suspensions were shaken at
 204 25 °C for 48 h at 170 rpm and then filtered for the measurement of total dissolved
 205 phosphorus (TDP), orthophosphate ($\text{PO}_4^{3-}\text{-P}$), total dissolved nitrogen (TDN),
 206 ammonia nitrogen ($\text{NH}_4^+\text{-N}$) and nitrate nitrogen ($\text{NO}_3^-\text{-N}$). Each experiment was
 207 carried out in triplicate.

208 **Table 2** Characteristics of the natural water used in the P adsorption experiment.

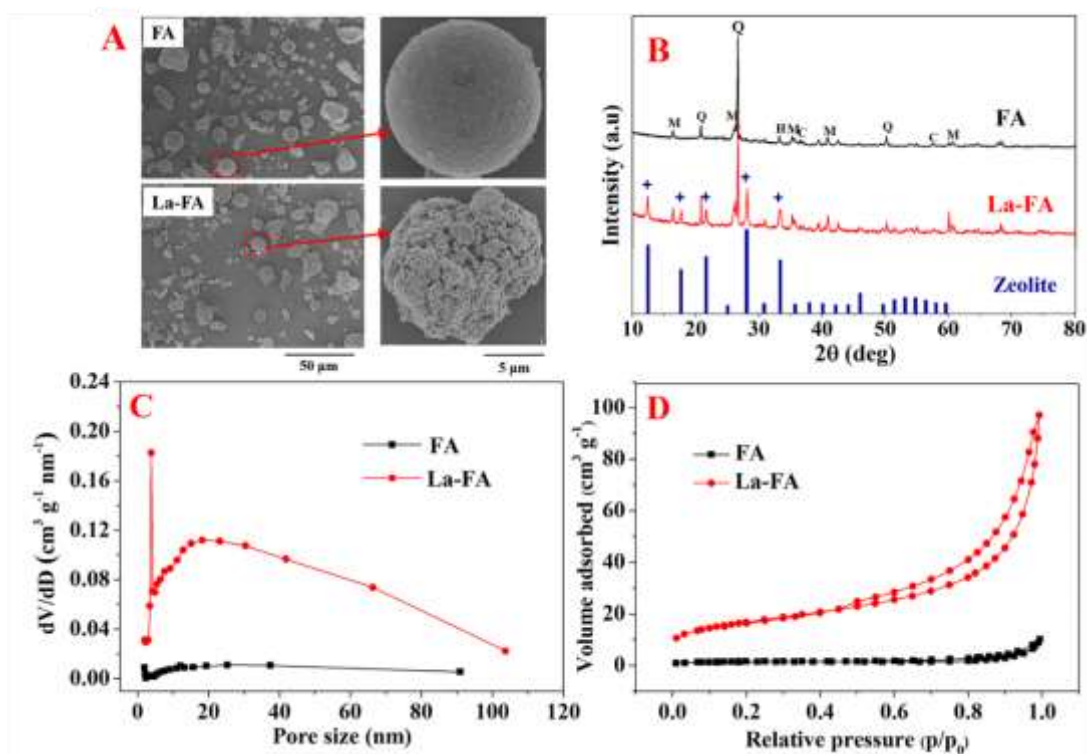
Parameter	Average value
pH	7.85
Dissolved oxygen (DO, $\text{mg O}_2 \text{ L}^{-1}$)	8.50
Electrical conductivity ($\mu\text{S cm}^{-1}$)	180
Total phosphorus (TP, mg P L^{-1})	0.067
Total dissolved phosphorus (TDP, mg P L^{-1})	0.030
Orthophosphate ($\text{PO}_4^{3-}\text{-P}$, mg P L^{-1})	0.011
Total nitrogen (TN, mg N L^{-1})	2.09
Total dissolved nitrogen (TDN, mg N L^{-1})	2.02
Nitrate nitrogen ($\text{NO}_3^-\text{-N}$, mg N L^{-1})	1.54
Ammonia nitrogen ($\text{NH}_4^+\text{-N}$, mg N L^{-1})	0.13
Dissolved organic carbon (DOC, mg L^{-1})	10.25

209 3. Results and discussion

210 3.1. Characterisation of the La-modified coal fly ash

211 The original FA particles were characterised by spherical morphologies and smooth
 212 surfaces, whereas particles of La-FA exhibited more irregular structures and much
 213 rougher surfaces (Fig. 1A). FESEM images indicated that particle size distributions of
 214 La-FA adsorbents were not uniform, with most average particle sizes of approximately
 215 20 μm . The proportion of La in La-FA was approximately 5.0% (w/w), which was
 216 slightly lower than that contained in the commercial La based P adsorbent, *Phoslock*[®]

217 (5.6%; Xu et al., 2017). These differences could be ascribed mainly to the formation of
 218 zeolite crystal clusters during the La modification process. XRD analysis (Fig. 1B)
 219 suggested that the original FA possessed crystalline phases of mullite ($3\text{Al}_2\text{O}_3 \cdot 2\text{SiO}_2$ or
 220 $2\text{Al}_2\text{O}_3 \cdot \text{SiO}_2$), quartz (SiO_4), hematite (Fe_2O_3) and corundum (Al_2O_3), which were also
 221 observed in the structures of La-FA. In addition, La-FA particles showed typical
 222 characteristic diffraction peaks similar to zeolite type Na-P1 ($\text{Na}_6\text{Al}_6\text{Si}_{10}\text{O}_{32} \cdot 12\text{H}_2\text{O}$,
 223 JCPDS code 39-0219) at $2\theta = 12.455^\circ$, 17.649° , 21.657° , 28.072° , and 33.356° .
 224 However, the characteristic diffraction peaks of La-(hydro)oxide were not detected in
 225 La-FA, possibly owing to its existence in an amorphous phase (Wang et al., 2016b).



226

227 **Fig. 1.** (A) SEM images of original FA and La-FA. (B) XRD patterns of original FA, La-FA,
 228 and zeolite identifying selected peaks of minerals quantified by Rietveld analysis (M = mullite,
 229 Q = quartz, H = hematite, C = corundum). (C) Pore size distribution of original FA and La-FA.

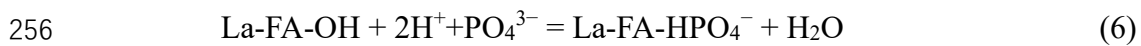
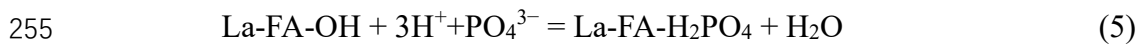
230 (D) N₂ adsorption/desorption isotherm of original FA and La-FA.

231 It has been reported that zeolite and hydrous La-oxide possesses a narrow pore size
232 distribution around 4.0 nm (Wang et al., 2016b). This data supports findings from this
233 study of a pore size distribution around 3.9 nm in La-FA (Fig. 1C), which was mainly
234 dependant on the pore structure of La-(hydro)oxide. The N₂ adsorption-desorption
235 isotherm of La-FA could be represented by a typical curve of type II (Fig. 1D). The
236 BET surface area of La-FA was measured at 59.9 m² g⁻¹, which was 10.9 times larger
237 than that of the original FA (5.5 m² g⁻¹), and in turn, was higher than that determined
238 for a lanthanum-doped coal fly ash-blast furnace cement composite with a surface area
239 of 11.4 m² g⁻¹ (Asaoka et al., 2020). Additionally, the pore volume of La-FA was
240 calculated to be 0.11 cm³ g⁻¹, which was 11.0-fold larger than that of the original FA
241 material, with a pore volume of 0.01 cm³ g⁻¹. Compared with the original FA, the
242 obvious increases in BET surface area and pore volume of La-FA have further
243 demonstrated the potential enhanced capabilities for P adsorption of the latter material.

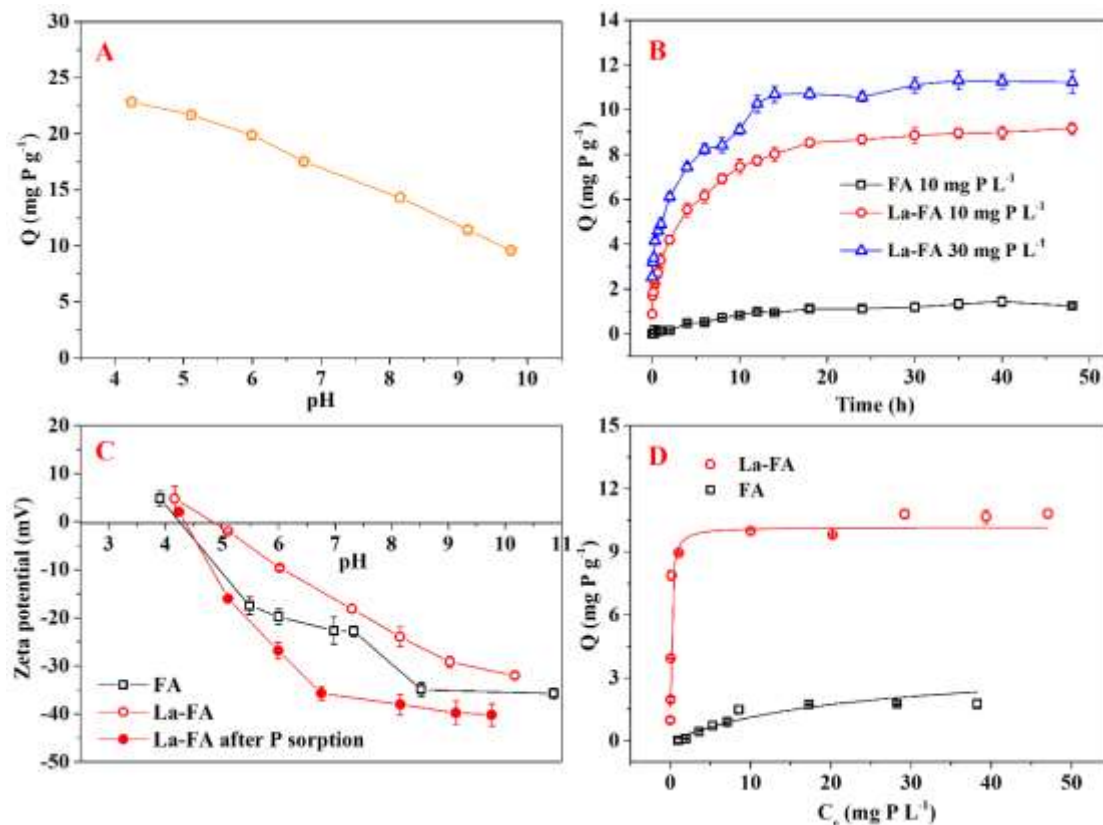
244 **3.2 P adsorption behaviours and mechanism**

245 At an initial P concentration of 30 mg P L⁻¹, La-FA exhibited the highest P adsorption
246 capacity of 22.8 mg P L⁻¹ at pH 4.25, which gradually decreased to 9.6 mg P L⁻¹ along
247 with increasing pH to 9.76 (Fig. 2A). The negative correlation between the P adsorption
248 capacity and pH was supported by previous relevant studies (Awual et al., 2011a;
249 Goscianska et al., 2017), and which may have been due to the increased hydroxide
250 concentration that might potentiate interference with the hard Lewis acid anion in water,

251 thus affecting P adsorption (Awual et al., 2011c). Moreover, hydrogen ions might
252 transfer to the surface of La-FA for capturing the dominant species of H_2PO_4^- and
253 HPO_4^{2-} according to the following reactions (Eq. 5) and (Eq. 6) (Awual et al., 2011b;
254 Hiemstra and Van Rimsdijk, 1996).



257 In order to simulate the scenario of P removal from eutrophic natural waters, a pH of
258 8.50 was chosen in the following experiments (Xiong & Peng, 2008). The capacities
259 for P adsorption, by the original FA and La-FA materials, increased with contact time
260 at initial P concentrations of 10 and 30 mg P L^{-1} and attained equilibrium after about 30
261 h (Fig. 2B). The pseudo-second order kinetics model better fitted the results (r^2 of
262 0.992-0.997) compared with those (r^2 of 0.886-0.936) obtained from the intra-particle
263 diffusion model (Table 3). The rate constants (k_2) of the original FA and La-FA were
264 calculated at 2.756 and 0.058 $\text{g mg}^{-1} \text{h}^{-1}$, under an initial P concentration of 10 mg L^{-1} ,
265 respectively. The rate constant for La-FA further decreased to 0.035 $\text{g mg}^{-1} \text{h}^{-1}$ when the
266 initial P concentration increased to 30 mg P L^{-1} .



267

268 **Fig. 2.** (A) Effect of pH on P adsorption efficiency for La-FA. (B) Kinetic studies for P
 269 adsorption by original FA and La-FA. (C) The ζ potentials of original FA, La-FA and La-FA
 270 after P adsorption. (D) Langmuir adsorption isotherms of P by original FA and La-FA.

271 **Table 3.** Pseudo-second order and intra-particle diffusion model parameters of P adsorption by
 272 original FA and La-FA.

Adsorbent	Initial P concentration (mg P L ⁻¹)	Pseudo-second order model			Intra-particle diffusion model	
		k_2 (g mg ⁻¹ h ⁻¹)	q_e (mg P g ⁻¹)	r^2	k_i (mg g ⁻¹ h ^{-1/2})	r^2
FA	10	2.756	0.378	0.992	0.236	0.936
La-FA	10	0.058	9.390	0.997	1.256	0.891
La-FA	30	0.035	13.141	0.992	1.354	0.886

273 The ζ potentials of original FA and La-FA materials exhibited decreasing trends with
 274 increasing pH value (Fig. 2C). The ζ potentials of La-FA were higher than those of the
 275 original FA under similar conditions of pH, possibly owing to the presence of La-

276 modified compounds (Goscianska et al., 2017). Additionally, the ζ potentials of La-FA
 277 after P adsorption all decreased compared to the initial values. For example, the initial
 278 ζ potential of La-FA was -24.0 mV at pH 8.15 and decreased to -38.1 mV after P
 279 adsorption. These results suggested that P might be bonded onto the surface of La-FA
 280 by formation of inner sphere complexes (Antelo et al., 2005; Wan et al., 2016).

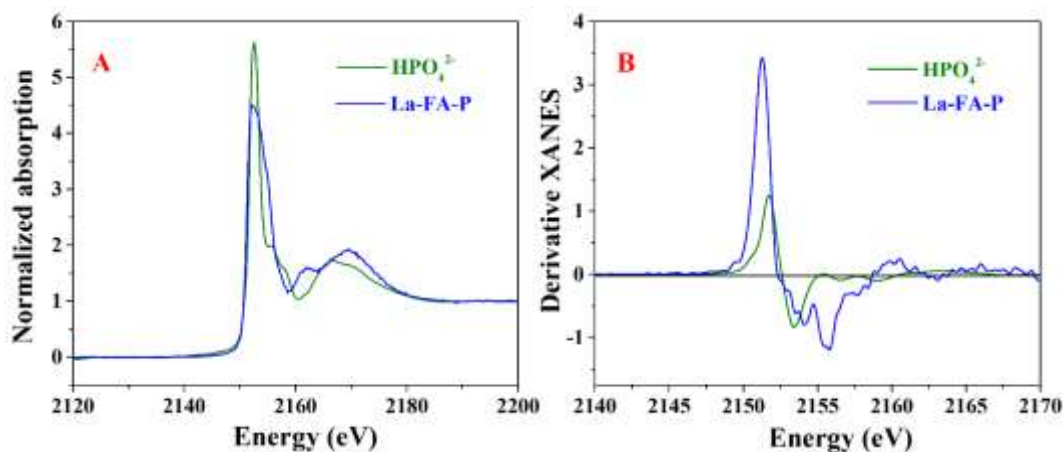
281 When evaluating the P adsorption capacity by La-FA compared to the original FA, a
 282 Langmuir isotherm model presented clearly better fittings (r^2 of 0.994-0.999) compared
 283 with those (r^2 of 0.713-0.831) fitted by the Freundlich model (Table 4). The better
 284 Langmuir isotherm simulation is visualised in Fig. 2D, and the maximum adsorption
 285 capacity of La-FA was determined to be 10.8 mg P g⁻¹, some 6.1 times higher than that
 286 of the original FA (1.8 mg P g⁻¹). In accordance with previous studies, the molar ratio
 287 of adsorbed P to La was used to calculate the efficiency of La usage in La-modified
 288 materials (Emmanuelawati et al., 2013; Yang et al., 2012; Yang et al., 2011). In the
 289 present study, the molar ratio of adsorbed P to La in La-FA was 0.96, by the ratio of the
 290 maximum amount of P adsorbed, calculated by the Langmuir model (10.8 mg P g⁻¹), to
 291 the total La content in La-FA (5.0%). The molar ratio of P to La (1:1) in the La-FA
 292 material was also in agreement with previous studies (Yasseri & Epe, 2015).

293 **Table 4.** Langmuir and Freundlich isotherms parameters of P adsorption by original FA and La-
 294 FA.

Adsorbent	Langmuir			Freundlich		
	q_m (mg P g ⁻¹)	k_L (L mg ⁻¹)	r^2	n	k_F (mg P g ⁻¹)	r^2

FA	1.752	1.675	0.994	0.895	0.002	0.831
La-FA	10.753	2.981	0.999	4.417	50.188	0.713

295 In order to investigate and demonstrate the mechanism at the molecular level, the P K-
296 edge XANES spectra of the La-FA sample containing bonded P was measured (Fig.
297 3A). As P has only one valance state, it can be perfectly characterised by the derivative
298 analysis of the XANES spectra (Khare et al., 2007). It has been reported that aqueous
299 Fe(III)–PO₄³⁻ solutions increased in the degree of bidentate compared to monodentate
300 bonding with increasing Fe/P ratio by using ferrihydrite adsorbent (Filatova et al., 1976).
301 However, in this study, there was no obvious change of white line energy from the La-
302 FA bonded P sample, compared to the derivative spectra for HPO₄²⁻ (Fig. 3B), possibly
303 indicating that P was bound on La-FA surfaces by adsorption (Khare et al., 2007).
304 Although XANES is recognized as an element-specific and in-situ method for the
305 detection of the molecular structures of reacting species (Khare et al., 2005; Xu et al.,
306 2017), it is beneficial to explore molecular mechanisms by combining the results from
307 multiple-characterisation methods, such as X-ray photoelectron spectroscopy (XPS),
308 and Fourier transform infrared spectroscopy (FTIR), which could be conducted in a
309 future study.



310

311 **Fig. 3.** (A) Normalized XANES spectra of HPO_4^{2-} and La-FA bonded with P. (B) First-

312 derivative XANES spectra for HPO_4^{2-} and La-FA bonded with phosphate.

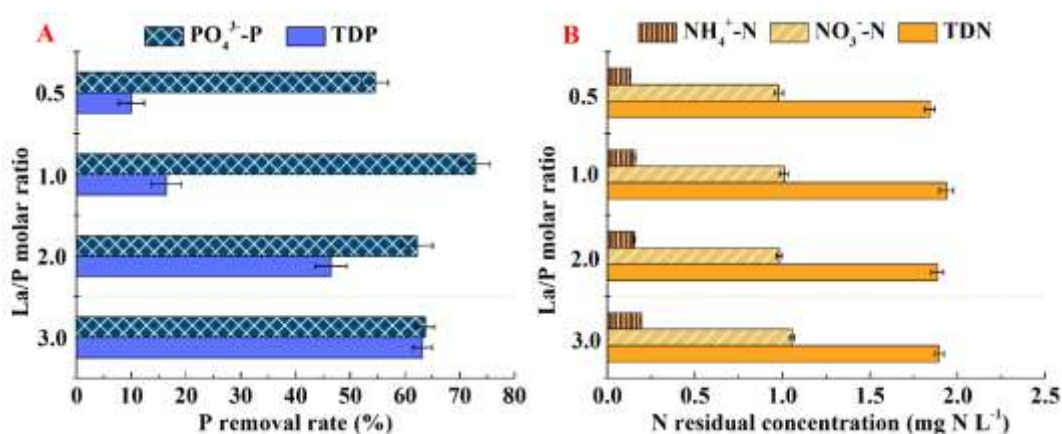
313 3.3. La-FA application in real natural waters

314 Previous studies have investigated the vertical distribution of La in-lake sediments for
 315 each experimental site, in order to explore the impact of *Phoslock*[®] being applied for
 316 remediation of eutrophic water bodies (Yasseri & Epe, 2015). Although the theoretical
 317 binding ratio of a La/P material was 1:1 based on the reaction equation ($\text{La}^{3+} + \text{PO}_4^{3-} =$
 318 LaPO_4), the application of materials with La/P molar ratios greater than 1:1 could
 319 increase P removal by up to 60% (Yasseri & Epe, 2015). Hence, it is suggested that
 320 more studies should be carried out in order to investigate the amount of La-modified
 321 material required in a real environmental application. Fig. 4 illustrates that the La-FA
 322 had a relatively efficient removal ability to PO_4^{3-} -P at different La/P molar ratios
 323 compared with TDP. With La/P molar ratios of 0.5:1, 1:1, 1.5:1 and 2:1, PO_4^{3-} -P
 324 removal efficiencies were $54.5 \pm 2.4\%$, $72.8 \pm 2.7\%$, $62.2 \pm 2.9\%$ and $63.6 \pm 1.8\%$,
 325 respectively. The La-FA material exhibited noticeably higher PO_4^{3-} -P removal ability
 326 with a La/P molar ratio of 1:1 compared with that a La/P molar ratio of 0.5:1, which

327 might suggest that this La/P molar ratio equalled the best theoretical value. Increasing
328 the La/P to 1.5:1 and further to 2:1 did not produce significant differences in the PO_4^{3-}
329 -P removal abilities, which might have been caused by saturation of adsorption sites in
330 the material. It should be noted that the current experiment was conducted in aqueous
331 solution without the presence of sediment. Taking into consideration P liberated from
332 sediments, higher dosage of La-modified materials might be applied in lake restoration
333 geo-engineering (Huang & Zhang, 2010). Nevertheless, the removal efficiency of TDP
334 by La-FA increased with increasing La/P molar ratio. In detail, the removal rate of TDP
335 was determined to be only $10.0 \pm 2.4\%$ with La/P molar ratio 0.5:1, but $63.2 \pm 1.8\%$
336 when the La/P molar ratio increased to 3:1 (Fig. 4A). In this study, La-FA exhibited
337 better selectivity to PO_4^{3-} -P than to TDP, possibly owing to presence of many other P
338 species (e. g. hexakisphosphate) in the latter (Wan et al., 2016).

339 Previous studies have demonstrated that some La-modified materials (e. g. La-
340 modified bentonite) could lead to adverse effects on the concentrations of nitrogen-
341 containing compounds in water (Reitzel et al., 2013). The nutrients, including NH_4^+ -N,
342 NO_3^- -N, and NO_2^- -N could attributed to the soluble fraction in the bentonite-based
343 material and to the nitrification process, as occurs in anaerobic sediments (Van
344 Oosterhout and Lüring, 2013; Gibbs et al., 2011). Such consequences might pose a risk
345 to the surface waters, as N is also one of the key causes of eutrophication (Wang et al.,
346 2016a; Zhang et al., 2018). In order to investigate the effect of La-FA material to
347 nitrogen in natural water system, we also determined the concentrations of NH_4^+ -N,
348 NO_3^- -N and TDN in water under different La-FA dosage regimes, which indicated that

349 La-FA had little effect on the nitrogen concentrations in water (Fig. 4B). With increase
 350 in La/P molar ratio, TDN content of the solution did not change significantly, compared
 351 with the initial concentration of 2.02 mg N L⁻¹ prior to adsorption (Table 2).
 352 Concentrations of NH₄⁺-N and NO₃⁻-N in the lake water was not noticeably affected by
 353 the addition of La-FA.



354
 355 **Fig. 4.** (a) Removal rates of PO₄³⁻-P and TDP by La-FA. (b) Residual concentrations of NH₄⁺-
 356 N, NO₃⁻-N and TDN after using La-FA.

357 3.4 Environmental implications

358 Laboratory experiments on La-FA have provided the theoretical basis and a technical
 359 reference for its further application in a natural aquatic environment. The key purpose
 360 of lake geological engineering is to control a eutrophication problem quickly and
 361 effectively (Reitzel et al., 2013). The maximum amount of P adsorbed by La-FA (10.8
 362 mg P g⁻¹, Fig. 4) was similar to that obtained by use of the commercially available
 363 material *Phoslock*[®] (10.6 mg P g⁻¹) (Haghseresht et al., 2009). However, as a material
 364 for the recapture of P for eutrophication control, the stability of the La-FA adsorbent
 365 should be considered when applied into natural waters. Here, La-FA showed great

366 ability to combine with P, exhibiting a desorption rate of 0.81% without taking into
367 consideration possible interference by submerged macrophytes in shallow waters
368 (Zhang et al., 2018). To the best of our knowledge, there exist many ionic species in
369 natural waters such as chloride, sulfate, calcium, magnesium, arsenic and nitrite (Shahat
370 et al., 2018; Awual, et al., 2019), which might act as potential antagonists for efficient
371 P adsorption. It has been reported that some hydrophobic materials, such as anion
372 exchange fibres prefer lowly hydrated anions (H_2PO_4^-) compared with highly hydrated
373 ones (H_2AsO_4^-) with the same electronic charge (Awual et al., 2008). In this study, as
374 an effective P adsorption material, La-FA showed better selectivity and sensitivity to
375 different P species for both synthetic and natural water systems (Fig. 4). However, the
376 effects of multiple different ions on efficiency of P removal by La-modified materials
377 should be further considered when applying these to natural waters. Based on the
378 current results of this study, longer-term experiments in large-scale systems should be
379 further conducted in order to better investigate the selectivity to different ions and to
380 evaluate the full cost-benefit of feasibility of waste utilization.

381 This study suggested that the proposed La-based material could provide a suitable
382 approach for the reuse of this type of industrial wastes. In addition to removal of P, La-
383 FA could provide a sediment covering function, possibly improving the anaerobic
384 environment of sediment and effectively slowing down the release of nutrients in
385 sediment. Practically, it would be necessary to determine the optimum dosage and
386 proportion of La-modified materials used for a project, according to the different
387 sediment environments present. As a natural lake system is very complex, investigation

388 into the specific effects of different dosages of La-modified materials on natural aquatic
389 organisms such as *Daphnia magna* and fish should be carried out. According to the
390 different water quality conditions and the types of aquatic organisms, the ecological
391 security of the aquatic organisms should be evaluated.

392 **4. Conclusions**

393 In this study, we have developed a La-modified adsorbent using solid waste coal fly ash
394 (La-FA) as raw material and investigated its performance for removal of phosphorus
395 from both synthetic and natural waters. The adsorption equilibrium data followed well
396 the Langmuir model with maximum adsorption capacity 10.8 mg P g⁻¹ of La-FA, some
397 6 times higher than that obtained from the original FA material. The pseudo-second-
398 order kinetic model was identified as the best model to describe the adsorption process.
399 Both the measurement of ζ potentials and P K-edge XANES spectra indicated that P
400 was probably bonded onto the La-FA by surface adsorption. The La-FA showed the
401 highest PO₄³⁻-P removal ability at a La/P molar ratio of 1:1. The application of La-FA
402 had negligible effects on the concentrations of TDN, NH₄⁺-N and NO₃⁻-N in water. With
403 these results, La-FA may be a potential material for the removal of P from polluted
404 natural waters for the mitigation of eutrophication.

405 **Declaration of competing interest**

406 The authors declare no conflicts of interest in this research.

407 **Acknowledgements**

408 This work was supported by National Key R&D Program of China (2017YFA0207204,

409 2018YFD0800305), National Natural Science Foundation of China (21377003), the
410 Major Science and Technology Program for Water Pollution Control and Treatment
411 (2018ZX07110004) and Joint Research Project for the Yangtze River Conservation
412 (Phase I, 2019-LHYJ-01).

413 **Reference**

414 Al-Mallahi, J., Sürmeli, R., Alli, B. 2020. Recovery of phosphorus from liquid digestate
415 using waste magnesite dust. *J. Clean. Prod.*, **272**, 122616.

416 Asaoka, S., Kawakami, K., Saito, H., Ichinari, T., Oikawa, T. 2020. Adsorption of
417 phosphate onto lanthanum-doped coal fly ash-Blast furnace cement composite.
418 *J. Hazard. Mater.*, **406**(2), 124780.

419 Awual, M. R., Asiri, A. M., Rahman, M. M., Alharthi, N. H. 2019. Assessment of
420 enhanced nitrite removal and monitoring using ligand modified stable conjugate
421 materials. *Chem. Eng. J.*, 363, 64-72.

422 Awual, M.R., El-Safty, S.A., Jyo, A. 2011a. Removal of trace arsenic (V) and phosphate
423 from water by a highly selective ligand exchange adsorbent. *J. Environ. Sci.*, **23**,
424 1947-1954.

425 Awual, M.R., Jyo, A. 2011b. Assessing of phosphorus removal by polymeric anion
426 exchangers. *Desalination*, **281**(1), 111-117.

427 Awual, M.R., Jyo, A., Ihara, T., Seko, N., Tamada, M., Him, K.T. 2011c. Enhanced trace
428 phosphate removal from water by zirconium (IV) loaded fibrous adsorbent. *Water*
429 *Res.*, **45**(15), 4592-4600.

430 Awual, M. R., Urata, S., Jyo, A., Tamada, M., & Katakai, A. 2008. Arsenate removal

431 from water by a weak-base anion exchange fibrous adsorbent. *Water Res.*, **42**(3),
432 689-696.

433 Barca, C., Gérente, C., Meyer, D., Chazarenc, F., Andres, Y. 2012. Phosphate removal
434 from synthetic and real wastewater using steel slags produced in Europe. *Water*
435 *Res.*, **46**(7), 2376-2384.

436 Biswas, B.K., Inoue, K., Ghimire, K.N., Harada, H., Ohto, K., H., K. 2008. Removal
437 and recovery of phosphorus from water by means of adsorption onto orange
438 waste gel loaded with zirconium. *Bioresource Technol.*, **99**, 8685-8690.

439 Blissett, R.S., Rowson, N.A. 2012. A review of the multi-component utilisation of coal
440 fly ash. *Fuel*, **97**, 1-23.

441 Bowden, L.I., Jarvis, A.P., Younger, P.L., Johnson, K.L. 2009. Phosphorus removal
442 from waste waters using basic oxygen steel slag. *Environ. Sci. Technol.*, **43**(7),
443 2476-2481.

444 Conley, D.J., Paerl, H.W., Howarth, R.W., Boesch, D.F., Seitzinger, S.P., Havens, K.E.,
445 Lancelot, C., Likens, G.E. 2009. Controlling eutrophication: nitrogen and
446 phosphorus. *Science*, **323**, 1014-1015.

447 Cy, A., Lpv, B. 2019. Wasted salted duck eggshells as an alternative adsorbent for
448 phosphorus removal. *J. Environ. Chem. Eng.*, **7**(6), 103443.

449 Dithmer, L., Nielsen, U.G., Lundberg, D., Reitzel, K. 2016. Influence of dissolved
450 organic carbon on the efficiency of P sequestration by a lanthanum modified
451 clay. *Water Res.*, **97**(Jun.15), 39-46.

452 Emmanuelawati, I., Yang, J., Zhang, J., Zhang, H.W., Zhou, L., Yu, C.Z. 2013. Low-

453 cost and large-scale synthesis of functional porous materials for phosphate
454 removal with high performance. *Nanoscale*, **5**(13), 6173-6180.

455 Fernandez, F.J., Villase, J., Rodriguez, L. 2007. Effect of the internal recycles on the
456 phosphorus removal efficiency of a WWTP. *Eng. Chem. Res.*, **46**, 7300-7307.

457 Filatova, L.N., Shelyakina, M.A., Plachinda, A.S., Makarov, E.F. 1976. Dimerisation
458 of iron (III) in aqueous solution in the presence of phosphate ions. *Russ. J. Inorg.
459 Chem.* **21**, 1494-1497.

460 Gibbs, M., M., Hickey, C., W., Özkundakci, D. 2011. Sustainability assessment and
461 comparison of efficacy of four P-inactivation agents for managing internal
462 phosphorus loads in lakes: sediment incubations. *Hydrobiologia*, **658**, 253-275.

463 Goscianska, J., Ptazkowska-Koniarz, M., Frankowski, M., Franus, M., Panek, R.,
464 Franus, W. 2017. Removal of phosphate from water by lanthanum-modified
465 zeolites obtained from fly ash. *J. Colloid Interf. Sci.*, **513**, 72-81.

466 Haghseresht, F., Wang, S., Do, D.D. 2009. A novel lanthanum-modified bentonite,
467 Phoslock, for phosphate removal from wastewaters *Appl. Clay Sci.*, **46**(4), 369-
468 375.

469 Hermassi, M., Valderrama, C., Font, O., Moreno, N., Cortina, J.L. 2020. Phosphate
470 recovery from aqueous solution by K-zeolite synthesized from fly ash for
471 subsequent valorisation as slow release fertilizer. *Sci. Total Environ.*, **731**,
472 139002.

473 Hiemstra, T., Van Rimsdijk, W.H. 1996. A surface structural approach to ion adsorption:
474 The charge distribution (CD) model. *J. Colloid Interface Sci.*, **179**, 488-508.

- 475 Huang, X.L., Zhang, J.Z. 2010. Spatial variation in sediment-water exchange of
476 phosphorus in Florida Bay: AMP as a model organic compound. *Environ. Sci.*
477 *Technol.*, **44**, 7790-7795.
- 478 Jano, P., Kopecká, A., Hejda, S. 2011. Utilization of waste humate product (iron humate)
479 for the phosphorus removal from waters. *Desalination*, **265**(1-3), 88-92.
- 480 Kang, S.K., Choo, K.H., Lim, K.H. 2003. Use of iron oxide particles as adsorbents to
481 enhance phosphorus removal from secondary wastewater effluent. *Sep. Sci.*
482 *Technol.*, **38**, 3853-3874.
- 483 Kasprzyk, M., Czerwionka, K., Gajewska, M. 2021. Waste materials assessment for
484 phosphorus adsorption toward sustainable application in circular economy.
485 *Resour. Conserv. Recy.*, **168**, 105335.
- 486 Khare, N., Hesterberg, D., Martin, J. D. 2005. XANES investigation of phosphate
487 sorption in single and binary systems of iron and aluminum oxide minerals.
488 *Environ. Sci. Technol.* **39** (7), 2152-2160.
- 489 Khare, N., Martin, J.D., Hesterberg, D. 2007. Phosphate bonding configuration on
490 ferrihydrite based on molecular orbital calculations and XANES fingerprinting.
491 *Geochim. Cosmochim. Ac.*, **71**(18), 4405-4415.
- 492 Kumar, P.S., Korving, L., Loosdrecht, M., Witkamp, G.J. 2019. Adsorption as a
493 technology to achieve ultra-low concentrations of phosphate: Research gaps and
494 economic analysis. *Water Research X*, **4**, 100029.
- 495 Lee, C.W., Kwon, H.B., Jeon, H.P., Koopman, B. 2009. A new recycling material for
496 removing phosphorus from water. *J. Clean. Prod.*, **17**, 683-687.

497 Li, Y.Z., Liu, C.J., Luan, Z.K., Peng, X.J., Zhu, C.L., Chen, Z.Y., Zhang, Z.G., Fan, J.H.,
498 Jia, Z.P. 2006. Phosphate removal from aqueous solutions using raw and activated
499 red mud and fly ash. *J. Hazard. Mater.*, **137**(1), 374-383.

500 Liu, D., Zhu, H., Wu, K., Wang, F., Liao, Q. 2020. Understanding the effect of particle
501 size of waste concrete powder on phosphorus removal efficiency. *Constr. Build.*
502 *Mater.*, **236**, 117526.

503 Nakarmi, A., Viswanathan, T., Bourdo, S.E., Watanabe, F., Moreira, R. 2020. Removal
504 and recovery of phosphorus from contaminated water using novel, reusable,
505 renewable resource-based Aluminum/Cerium oxide nanocomposite. *Water Air*
506 *Soil Poll.*, **231**, 559.

507 Pan, G., Lyu, T., Mortimer, R. 2018. Comment: closing phosphorus cycle from natural
508 waters: re-capturing phosphorus through an integrated water-energy-food
509 strategy. *J. Environ. Sci.*, **65**, 375-376.

510 Pan, G., Miao, X.J., Bi, L., Zhang, H.G., Wang, L., Wang, L.J., Wang, Z.B., Chen, J.,
511 Ali, J., Pan., M.M., Zhang, J., Yue, B., Lyu, T. 2019. Modified local soil (MLS)
512 technology for harmful algal bloom control, sediment remediation, and ecological
513 restoration. *Water*, **11**(6):1123.

514 Pan, M., Tao, L., Zhang, M., Zhang, H., Pan, G. 2020. Synergistic Recapturing of
515 External and Internal Phosphorus for In Situ Eutrophication Mitigation. *Water*,
516 **12**(1), 2.

517 Ravel, B., Newville, M. 2005. ATHENA, ARTEMIS, HEPHAESTUS: data analysis for
518 X-ray absorption spectroscopy using IFEFFIT. *J. Synchrotron Radiat.*, **12**, 537-

519 541.

520 Reitzel, K., Lotter, S., Dubke, M., Egemose, S., Jensen, H.S., Andersen, F.Ø. 2013.

521 Effects of Phoslock treatment and chironomids on the exchange of nutrients

522 between sediment and water. *Hydrobiologia*, **703**(1), 189-202.

523 Shahat, A., Hassan, M.A., El-Shahat, M.F., Shahawy, O.E., Awual, M. R. 2018. Visual

524 nickel (II) ions treatment in petroleum samples using a mesoporous composite

525 adsorbent. *Chem. Eng. J.*, **334**, 957-967.

526 Shin, E.W., Karthikeyan, K.G., Tshabalala, M.A. 2005. Orthophosphate sorption onto

527 lanthanum-treated lignocellulosic sorbents. *Environ. Sci. Technol.*, **39**(16),

528 6273-6279.

529 Shuai Gu, Bitian Fu, Ji-Whan Ahn, Fang, B.Z. 2021. Mechanism for phosphorus

530 removal from wastewater with fly ash of municipal solid waste incineration,

531 Seoul, Korea. *J. Clean. Prod.*, **280**, 124430.

532 Smith, V.H., Tilman, G.D., Nekola, J.C. 1999. Eutrophication: impacts of excess

533 nutrient inputs on freshwater, marine, and terrestrial ecosystems. *Environ.*

534 *Pollut.*, **100**, 179-196.

535 Torit, J., Pihusut, D. 2019. Phosphorus removal from wastewater using eggshell ash.

536 *Environ. Sci. Pollut. Res.*, **26**, 34101-34109.

537 Van, Oosterhout, F., Lüring, M. 2013. The effect of phosphorus binding clay

538 (Phoslock®) in mitigating cyanobacterial nuisance: a laboratory study on the effects

539 on water quality variables and plankton. *Hydrobiologia*, **710**, 265-277.

540 Vassilev, S.V., Vassileva, C.G. 2005. Methods for characterization of composition of fly

541 ashes from coal-fired power stations: a critical overview. *Energy Fuels*, **19**(3),
542 1084-1098.

543 Wan, B., Yan, Y., Fan, L., Tan, W., He, J., Feng, X. 2016. Surface speciation of myo-
544 inositol hexakisphosphate adsorbed on TiO₂ nanoparticles and its impact on
545 their colloidal stability in aqueous suspension: A comparative study with
546 orthophosphate. *Sci. Total Environ.*, **544**(feb.15), 134-142.

547 Wang, L.J., Pan, G., Shi, W.Q., Wang, Z.B., Zhang, H.G. 2016a. Manipulating nutrient
548 limitation using modified local soils: a case study at Lake Taihu (China). *Water*
549 *Res.*, **101**, 25-35.

550 Wang, Z., Dong, J., Liu, L., Zhu, G., Liu, C. 2013. Screening of phosphate-removing
551 substrates for use in constructed wetlands treating swine wastewater. *Ecol. Eng.*,
552 **54**, 57-65.

553 Wang, Z., Fan, Y., Li, Y.W., Qu, F.R., Wu, D.Y., Nan, K.H. 2016b. Synthesis of
554 zeolite/hydrous lanthanum oxide composite from coal fly ash for efficient
555 phosphate removal from lake water. *Micropor. Mesopor. Mat.*, **222** 226-234.

556 White, S.A., Strosnider, W., Chase, M., Schlautman, M.A. 2021. Removal and reuse of
557 phosphorus from plant nursery irrigation return water with reclaimed iron
558 oxides. *Ecol. Eng.*, **160**(1), 106153.

559 Xiong, J., Qin, Y., Islam, E., Yue, M., Wang, W. 2011. Phosphate removal from solution
560 using powdered freshwater mussel shells. *Desalination*, **276**, 317-321.

561 Xiong, W.H., Peng, J. 2008. Development and characterization of ferrihydrite-modified
562 diatomite as a phosphorus adsorbent. *Water Res.*, **42**, 4869-4877.

563 Xu, R., Tao, L., Zhang, M., Cooper, M., Pan, G. 2020. Molecular-level investigations
564 of effective biogenic phosphorus adsorption by a lanthanum/aluminum-
565 hydroxide composite. *Sci. Total Environ.*, **725**, 138424.

566 Xu, R., Zhang, M.Y., Mortimer, R., Pan, G. 2017. Enhanced phosphorus locking by
567 novel lanthanum/aluminum-hydroxide composite: implications for
568 eutrophication control. *Environ. Sci. Technol.*, **51**, 3418-3425.

569 Yang, J., Yuan, P., Chen, H.Y., Zou, J., Yuan, Z.G., Yu, C.Z. 2012. Rationally designed
570 functional macroporous materials as new adsorbents for efficient phosphorus
571 removal. *J. Mater. Chem.*, **22**(19), 9983-9990.

572 Yang, J., Zhou, L., Zhao, L.Z., Zhang, H.W., Yin, J., Wei, G.F., Qian, K., Wang, Y.H.,
573 Yu, C.Z. 2011. A designed nanoporous material for phosphate removal with high
574 efficiency. *J. Mater. Chem.*, **21**(8), 2489-2494.

575 Yasserli, S., Epe, T.S. 2015. Analysis of the La:P ratio in lake sediments-Vertical and
576 spatial distribution assessed by a multiple-core survey. *Water Res.*, **97**, 96-100.

577 Zamparas, M., Kyriakopoulos, G.L., Drosos, M., Kapsalis, V.C., Kalavrouziotis, I.K.
578 2020. Novel composite materials for lake restoration: A new approach
579 impacting on ecology and circular economy. *Sustainability*, **12**(8), 3397.

580 Zhang, H.G., Shang, Y.Y., Lyu, T., Chen, J., Pan, G. 2018. Switching harmful algal
581 blooms to submerged macrophytes in shallow waters using geo-engineering
582 methods: evidence from a ¹⁵N tracing study. *Environ. Sci. Technol.*, **52**, 11778-
583 11785.

584 Zhang, Y., Pan, B., Chao, S., Xiang, G. 2016. Enhanced phosphate removal by

585 nanosized hydrated La(III) oxide confined in cross-linked polystyrene networks.

586 *Environ. Sci. Technol.*, **50**(3), 1447.